NeuroImage: Clinical 33 (2022) 102938

Contents lists available at ScienceDirect

NeuroImage: Clinical

journal homepage: www.elsevier.com/locate/ynicl

R2* relaxometry analysis for mapping of white matter alteration in Parkinson's disease with mild cognitive impairment

Hirohito Kan [a,b,*], Yuto Uchida [c,d], Yoshino Ueki [e], Nobuyuki Arai [f], Satoshi Tsubokura [g], Hiroshi Kunitomo [g], Harumasa Kasai [g], Kiminori Aoyama [e], Noriyuki Matsukawa [c], Yuta Shibamoto [b]

[a] Department of Integrated Health Sciences, Nagoya University Graduate School of Medicine, Japan
[b] Department of Radiology, Nagoya City University, Graduate School of Medical Sciences, Japan
[c] Department of Neurology, Nagoya City University, Graduate School of Medical Sciences, Japan
[d] Department of Neurology, Toyokawa City Hospital, Japan
[e] Department of Rehabilitation Medicine, Nagoya City University, Graduate School of Medical Sciences, Japan
[f] Department of Radiology, Suzuka University of Medical Science, Japan
[g] Department of Radiology, Nagoya City University Hospital, Japan

ARTICLE INFO

Keywords:
Parkinson's disease
R2* relaxometry analysis
Quantitative susceptibility mapping
Voxel-based analysis
PD-MCI

ABSTRACT

Background: R2* relaxometry analysis combined with quantitative susceptibility mapping (QSM), which has high sensitivity to iron deposition, can distinguish microstructural changes of the white matter (WM) and iron deposition, thereby providing a sensitive and biologically specific measure of the WM owing to the changes in myelin and its surrounding environment. This study aimed to explore the microstructural WM alterations associated with cognitive impairment in patients with Parkinson's disease (PD) using R2* relaxometry analysis combined with QSM.

Materials and methods: We enrolled 24 patients with PD and mild cognitive impairment (PD-MCI), 22 patients with PD and normal cognition (PD-CN), and 19 age- and sex-matched healthy controls (HC). All participants underwent Montreal Cognitive Assessment (MoCA) and brain magnetic resonance imaging, including structural three-dimensional T1-weighted images and multiple spoiled gradient echo sequence (mGRE). The R2* and susceptibility maps were estimated from the multiple magnitude images of mGRE. The susceptibility maps were used for verifying iron deposition in the WM. The voxel-based R2* of the entire WM and its correlation with cognitive performance were analyzed.

Results: In the voxel-based group comparisons, the R2* in the PD-MCI group was lower in some WM regions, including the corpus callosum, than R2* in the PD-CN and HC groups. The mean susceptibility values in almost all brain regions were negative and close-to-zero values, indicating no detectable paramagnetic iron deposition in the WM of all subjects. There was a significant positive correlation between R2* and MoCA in some regions of the WM, mainly the corpus callosum and left hemisphere.

Conclusion: R2* relaxometry analysis for WM microstructural changes provided further biologic insights on demyelination and changes in the surrounding environment, supported by the QSM results demonstrating no iron existence. This analysis highlighted the potential for the early evaluation of cognitive decline in patients with PD.

1. Introduction

About 50% of patients with Parkinson's disease (PD) show dementia, even in the early disease stage (Muslimovic et al., 2005). A large number of patients with PD have a subtle cognitive decline, which is called PD with mild cognitive impairment (PD-MCI) and has a potential risk for

* Corresponding author at: Department of Integrated Health Sciences, Nagoya University Graduate School of Medicine, Japan.
E-mail addresses: kan@met.nagoya-u.ac.jp (H. Kan), uchidayuto0720@yahoo.co.jp (Y. Uchida), yueki@med.nagoya-cu.ac.jp (Y. Ueki), arai@suzuka-u.ac.jp (N. Arai), ra110801@med.nagoya-cu.ac.jp (S. Tsubokura), rakunny@med.nagoya-cu.ac.jp (H. Kunitomo), norim@med.nagoya-cu.ac.jp (N. Matsukawa), yshiba@med.nagoya-cu.ac.jp (Y. Shibamoto).

https://doi.org/10.1016/j.nicl.2022.102938
Received 20 August 2021; Received in revised form 22 December 2021; Accepted 3 January 2022
Available online 4 January 2022

conversion to PD dementia. The severity of cognitive decline and onset of PD-MCI are widely known to vary considerably (Lanskey et al., 2018). The cognitive decline in PD is partly caused by changes in neurotransmitters, such dopamine, acetylcholine, serotonin, and norepinephrine, which are essential for passing on information among neurons (Kehagia et al., 2010). Despite the clinical importance of PD-MCI, the neuropathologic basis has not been fully understood. Accurate diagnosis of PD-MCI is clinically essential for a healthcare plan that would retard the progression of cognitive decline and for clarification of the underlying mechanism of disease development.

White matter (WM) alteration is potentially sensitive to the early processes, such as degeneration of axon and myelin damage, in PD (Burke and O'Malley, 2013; Rektor et al., 2018) and may develop secondary to neural network disruption in neurotransmitters. Several studies on patients with PD reported that diffusion tensor imaging (DTI) allowed identification of microstructural alterations in WM, with results that were linked with the cognitive deficits. (Agosta et al., 2014; Bledsoe et al., 2018; Guimarães et al., 2018; Hattori et al., 2012; Kamagata et al., 2013; Kim et al., 2013; Zarkali et al., 2020; Zheng et al., 2014). Although the reported presence and location of fractional anisotropy (FA) and mean diffusivity (MD) changes varied across studies, such WM alterations included decrease in FA and/or increase in MD. However, these diffusion-based metrics are relatively more sensitive to the axon density, cell swelling, fiber structure, and axon radius (Beaulieu, 2009). DTI analysis is sensitive, but it has definite limitations for an accurate assessment of tissue microstructural status, because DTI exerts its abovementioned effects as an indirect biomarker through water molecular diffusion. To overcome this problem, another WM-sensitive quantification method that can verify the pathologic WM changes is needed.

R2* relaxometry analysis has been utilized to evaluate iron deposition from multiple spoiled gradient echo sequence (mGRE) (Song et al., 2008). Besides the estimation of iron deposition, R2* value is also sensitive to the microstructural changes of the WM (Paling et al., 2012). The myelin water fraction using multicomponent R2* relaxometry analysis (Du et al., 2007) has been developed to directly quantify myelin and has attracted considerable attention as an *in vivo* imaging biomarker of myelin because its values were found to be reasonably correlated with histologic measurements (Laule et al., 2008). Even simple R2* relaxometry analysis may be reflective of the microstructural changes of the WM, including myelin loss in WM alteration. On the other hand, quantitative susceptibility mapping (QSM) is an advanced quantitative technique that has high sensitivity to iron deposition. Therefore, R2* relaxometry analysis combined with QSM may distinguish microstructural changes and iron deposition, thereby providing a biologically specific measure of the WM and aiding in understanding the pathological changes of WM in PD-MCI. We hypothesized that decrease in R2* may be observed owing to demyelination followed by alterations in surrounding conditions, which are involved in WM alteration in patients with PD-MCI.

To investigate the WM alterations associated with cognitive impairment in patients with PD, we performed voxel-based R2* relaxometry analysis in patients with PD-MCI, PD with normal cognition (PD-CN), and healthy controls (HC) and evaluated the relationship between R2* value and cognitive performance in patients with PD.

2. Material and methods

2.1. Participants

This cross-sectional study on clinical and quantitative neuroimaging markers enrolled patients with PD-MCI, PD-CN, and HC. We enrolled 24 patients with PD-MCI (72.4 ± 6.1 years old, 13 men and 11 women), 22 patients with PD-CN (70.8 ± 5.9 years old, 12 men and 10 women), and 19 age- and sex-matched HC (71.4 ± 5.3 years old, 10 men and 9 women). All participants fulfilled the following inclusion criteria: age > 50 years, clinical dementia rating < 1, and Hoehn and Yahr stage < 5. The exclusion criteria were any history of head trauma, cerebrovascular disease, deep and subcortical WM magnetic resonance imaging (MRI) hyperintensities > Fazekas grade (Fazekas et al., 1987) 2, metabolic disease, or severe psychiatric illness. The purpose and procedures associated with our investigations were fully explained to the participants, and the studies were performed only after obtaining informed consent from each participant. This study was approved by the institutional review board of Nagoya City University Hospital and Nagoya University.

2.2. Clinical and cognitive evaluations

Participants with PD-MCI and PD-CN had discontinued antiparkinsonian medications for at least 12 h before undergoing evaluation with the Movement Disorder Society Unified Parkinson's Disease Rating Scale motor part III (MDS-UPDRS part III). Then, the patients underwent the Montreal Cognitive Assessment (MoCA) (Dalrymple-Alford et al., 2010) as a global cognitive assessment tool. Moreover, the MoCA subscores related to language were also evaluated. In addition, the clinical dementia rating, the digit span backward, and the Stroop Color and Word test were performed to screen the executive function. The Stroop Color and Word test card consists of 80 items organized in a 10-line by 8-column matrix. In the Stroop Color and Word test, the participant is required to name the color of the printed word, which is incongruent, and the completion time is recorded (Litvan et al., 2011). Notably, the MoCA and other tests were completed in the on-medication state. The clinical diagnosis of PD-MCI was made according to the MDS Task Force level 1 criteria (Litvan et al., 2012) as follow: (1) objective cognitive deficits with scores at least 2.0 standard deviations below the mean of controls on the MoCA or two or more cognitive domains within a limited battery of neuropsychological tests and (2) subjective cognitive decline reported by the patient or their family members with a score of 1 or higher on item 1 (cognitive impairment) of the MDS-UPDRS part I. Participants with PD without dementia who did not meet the MDS Task Force level 1 criteria for PD-MCI were classified as PD-CN.

2.3. Magnetic resonance imaging experiments

All subjects were scanned using a 3 T magnetic resonance imaging scanner (Magnetom Skyra, Siemens Healthcare, Erlangen, Germany). Three-dimensional (3D) mGRE was acquired in the axial plane and precisely perpendicular to the static magnetic field. Right-left phase encoding and anterior-posterior frequency encoding were used. The scan parameters for mGRE were as follows: FOV, 192 × 192 × 160 mm^3; matrix size, 192 × 192 × 160; TR, 36 ms; TE, 6.4–32.0 ms at 6.4-ms intervals; number of echoes, 5; parallel imaging factor, 2; and flip angle, 15°. To spatially normalize and perform voxel-based morphometry (VBM), the 3D T1-weighted images were acquired by magnetization-prepared rapid acquisition with a gradient echo sequence (MPRAGE) in the sagittal plane and with the following scan parameters: FOV, 256 × 256 × 176 mm^3; matrix size, 256 × 256 × 176; TR, 7.3 ms; TE, 2.4 ms; inversion time, 900 ms; interval between successive inversion pulses, 1900 ms; parallel imaging factor, 2; and flip angle, 9°. T2-weighted turbo spin echo, fluid-attenuated inversion recovery, diffusion-weighted, and T2*-weighted images were acquired routinely to exclude any brain abnormalities.

2.4. R2* relaxometry analysis

To investigate microstructural WM changes, R2* (reciprocal of T2*) relaxometry analysis was performed using multiple magnitude and phase images that were acquired from the mGRE sequence (Sedlacik et al., 2014). Prior to mGRE-based R2* decay estimation, the signal correction was performed by the following steps, because the signal of mGRE is sensitive to excessive signal loss secondary to a macroscopic field inhomogeneity (Alonso-Ortiz et al., 2017). The phase images in

each TE was unwrapped using quality-guiled phase unwrapping (Fortier and Levesque, 2018). The unwrapped phase images were performed by linear fitting to determine the total field map. The background field was estimated from the total field map using regularization-enabled sophisticated harmonic artifact reduction for phase data with varying kernel sizes (Kan et al., 2016). For each pixel, the first order approximations of the background field gradients in x, y, and z directions were determined using the corresponding differences between neighboring voxels. To correct the signal loss in the magnitude images, we used 3D signal correction with a sinc function and the first order approximation of the background field gradient (Alonso-Ortiz et al., 2017; Dahnke and Schaeffter, 2005; Hwang et al., 2010), as expressed by Eq. (1)

$$S_i = S_{i,c} * sinc\left(\gamma G_x \frac{\Delta x}{2} TE_i\right) * sinc\left(\gamma G_y \frac{\Delta y}{2} TE_i\right) * sinc\left(\gamma G_z \frac{\Delta z}{2} TE_i\right) \quad (1)$$

where S_i and $S_{i,\,c}$ are the original and corrected signal intensities at TE_i, respectively; γ is the gyromagnetic rotation ratio; and $G_{x,\,y,\,z}$, and $\Delta x,\, y,\, z$ are the linear approximations of the background field gradients and the voxel sizes in the x, y, and z directions, respectively.

The R2* value was fitted from the multiple magnitude data to the mono-exponential R2* decay using auto-regression on linear operations (Pei et al., 2015), which provides fast and accurate R2* estimation using maximum-likelihood fit of an autoregressive model (ALRO). As the WM signal comprises multiple components and shim variations, it was necessary to investigate whether the mono-exponential decay model can sufficiently explain the signal decay by estimating the fitting error. The fitting error map of the mono-exponential R2* decay model was estimated by Eq. (2)

$$Fitting\ \ error = \frac{\sum_{i=1}^{N} \sqrt{\left(\frac{S_{TE_i} - S_{0,fit} e^{-R^*_{2,fit} TE_i}}{S_{TE_i}}\right)^2}}{N} \quad (2)$$

where S_{TEi} is the signal intensity corrected field inhomogeneity at each TE; N is the number of TE; and $S_{0,fit}$ and $R^*_{2,\,fit}$ are the signal intensity at TE = 0 and the R2* value calculated by the ARLO algorithm.

2.5. QSM analysis for the evaluation of iron deposition in WM

To confirm whether iron deposition can be attributed to R2* value changes, we used QSM analysis, which is a quantification method that has excellent sensitivity to the presence of iron and enables estimation of the susceptibility within a voxel (Deistung et al., 2017). In this study, the QSM analysis in WM used for only verifying detectable iron deposition in WM because there was a relatively small difference in the susceptibility between HCs and patients with PD (Guan et al., 2019). Notably, the aim of the QSM analysis was not to find significant differences between groups.

Laplacian-based unwrapping was applied on the phase images of mGRE (Bagher-Ebadian et al., 2008). Each unwrapped phase was removed by the background field using the sophisticated harmonic artifact reduction for phase data with varying kernel sizes (Özbay et al., 2017). Weighted averaging was performed on the local fields of each TE, based on the T2* map estimated from the magnitude images (Wu et al., 2012). The susceptibility map was reconstructed from the local field map using the improved sparse linear equations and least square method (Kan et al., 2017; Li et al., 2015). The lateral ventricle mean CSF susceptibility extracted from the T2* map was used as a zero reference of susceptibility value (Kan et al., 2020).

2.6. Voxel-based analyses of R2* and WM volume among groups

The T1-weighted structural images acquired from MPRAGE were used for the VBM of WM and were segmented into three classes (i.e., GM, WM, and CSF) on statistical parametric mapping 12 (SPM12). The WM images were transformed into Montreal Neurologic Institute (MNI) space for spatial normalization using a study-specific template generated by diffeomorphic anatomical registration using the exponentiated Lie algebra algorithm (Ashburner, 2007). This image was smoothed using an isotropic 8-mm Gaussian kernel and modulated to preserve brain volume. We used the masking toolbox on the SPM12 to make the WM mask for VBM (Ridgway et al., 2009). The magnitude image of the first TE in the mGRE was coregistered between the above T1-weighted structural images that were used for VBM. The R2* map was transformed into MNI space using the same transformation parameter for spatial normalization. The normalized quantitative images were smoothed using an isotropic 8-mm Gaussian kernel.

In voxel-based R2* analysis, the groups were compared in terms of the covariates of age, sex, education, and orientations of the head against the main magnetic field (i.e., pitch and yaw). The reason for including the directions of the head as covariates was based on the influence of the myelin fiber orientation against the main magnetic field on the R2* (Kor et al., 2019; Sedlacik et al., 2014). The whole WM volume comparison was performed in terms of covariates of age, sex, and education. In voxel-based WM volume, the individual differences in WM volume were statistically controlled using the total WM volume of each participant to determine the regional volume decrease. The WM atlas made by Johns Hopkins University (JHU-WM atlas) (Mori et al., 2008) was used to identify the anatomical regions, which reached significance in the voxel-based analyses.

2.7. Relationship between R2* and susceptibility

To provide additional insight into the nature of WM changes, ROI analyses were performed to find the relationship between both indices. To determine the relationship between R2* relaxometry and QSM, we measured the mean values in the spatially normalized R2* and susceptibility maps without smoothing the steps in the splenium of the corpus callosum, which was the representative region mapped in the JHU-WM atlas. The abnormality of diffusion-based metrics was reported in the splenium of the corpus callosum in PD (Georgiopoulos et al., 2017). Moreover, the iron deposition was evaluated using the mean susceptibility value in the spatially normalized susceptibility map without smoothing using the volume of interests mapped by the JHU-WM atlas.

2.8. Statistical analysis

All statistical analyses were performed using IBM SPSS Statistics for Windows, version 26.0 (IBM Corporation, Armonk, NY, USA), except for the whole-brain voxel-based and correlation analyses described below, which were performed using SPM12.

The clinical characteristics were presented as mean values and were compared among the three groups using one-way analysis of variance with posthoc test and Bonferroni correction for multiple comparisons. Sex was compared using Chi-square test. Bonferroni-corrected $P < 0.05$ was considered statistically significant. To determine group differences in R2* and WM volume, voxel-wise comparisons of the covariance tests were performed. The statistical significance level was set as the family-wise error (FWE)-corrected $P < 0.05$ at the cluster-wise level.

The relationship between susceptibility and R2* was determined via bivariate correlation analysis using Pearson product-moment correlation coefficient with the splenium of the corpus callosum as the representative region.

To assess the relationship between cognition and R2*, we performed voxel-wise correlation of covariance test. A statistical significance level of $P < 0.05$ was applied, with FWE correction at the cluster-wise level. In addition, to obtain an overview of these correlations, partial correlation analyses were performed to scrutinize the regional correlation of MoCA with R2* in the representative regions based on correlation analysis. Note that the effects of age, sex, education, and orientations of the head against the main magnetic field (for only R2*) were removed from the MoCA and R2* values measured using the volume of interests mapped

by the JHU-WM atlas.

3. Results

3.1. Comparisons of the neuroimaging features and demographic characteristics

The clinical characteristics of the study population are shown in Table 1. The participants were matched by age ($P = 0.66$), sex ($P = 0.91$), and education duration ($P = 0.29$). The PD-MCI and PD-CN groups had no significant differences in disease duration ($P = 0.90$), Hoehn and Yahr stage ($P = 0.26$), MDS-UPDRS part III off-state ($P = 0.71$), levodopa-equivalent dose ($P = 0.67$), digit span backward tests ($P = 0.08$), and total intracranial volume ($P = 0.039$) but had significant differences in MoCA ($P < 0.001$), Stroop interference test ($P < 0.01$), whole WM ($P < 0.05$), and total brain volumes ($P < 0.01$). Additionally, the MoCA subscores related to language functions, such as repeat sentences and categorical naming tests, were lower in the PD-MCI group than those in the PD-CN group ($P < 0.001$). The head orientations against the static magnetic field did not differ among the groups ($P = 0.07$ and 0.36 in pitch and yaw, respectively).

3.2. Group differences in R2* and WM volume among groups

The representative images of R2*, fitting error in the R2* decay model, susceptibility, and color susceptibility maps in the PD-MCI, PD-CN, and HC groups are depicted in Fig. 1. The fitting error maps represent a white-noise-like pattern, except around the blood vessels. The mean error was around 1 % throughout the brain. In the voxel-based R2* comparisons among the groups, the R2* value in the PD-MCI group was significantly lower in several WM regions, including the corpus callosum, than the R2* values in the PD-CN and HC groups (both FWE-corrected $P < 0.05$; Fig. 2a, b). VBM showed no differences in WM atrophy between the patients with PD and HCs. The significant regions in the voxel-based group comparison are summarized in Table 2.

Table 1
Comparisons of the neuroimaging features and demographic characteristics among the participants.

	PD-MCI	PD-CN	HC	*P* value
n [male/female]	24 [13/11]	22 [12/10]	19 [10/9]	ns
Age (years)	72.4 (6.1)	70.8 (5.9)	71.4 (5.3)	ns
Education (years)	11.7 (2.4)	12.3 (2.1)	12.7 (2.2)	ns
Disease duration (years)	7.2 (4.4)	7.3 (3.4)	NA	ns
Hoehn and Yahr stage	2.5 (0.5)	2.3 (0.6)	NA	ns
UPDRS-III off-state	28.6 (13.7)	27.0 (15.3)	NA	ns
LEDD (mg)	378.0 (136.4)	359.6 (155.9)	NA	ns
MoCA-total	21.6 (1.9)	27.8 (2.4)	28.7 (1.0)	<0.001 a, b
MoCA-language	1.5 (0.9)	2.4 (0.7)	2.5 (0.6)	<0.001 a, b
Digit span backward	3.7 (1.8)	4.5 (2.0)	4.9 (1.9)	ns
Stroop interference	88.2 (41.3)	70.5 (31.5)	56.2 (21.1)	0.009b
Pitch (°)	14.2 (9.4)	12.9 (8.3)	8.5 (5.7)	ns
Yaw (°)	2.3 (1.1)	2.8 (1.9)	2.2 (1.2)	ns
WMV (mL)	386.70 (84.6)	438.5 (59.3)	415.1 (48.1)	0.039 a
TBV (mL)	911.4 (109.1)	1015.2 (120.8)	1000.0 (84.2)	0.003 a, b
TIV (mL)	1410.5 (146.3)	1468.0 (152.3)	1429.9 (126.6)	ns

Data presented as mean (standard deviation).
[a]PD-MCI < PD-CN (Bonferroni-corrected $P < 0.05$).
[b]PD-MCI < HC (Bonferroni-corrected $P < 0.05$).
[c]PD-CN < HC (Bonferroni-corrected $P < 0.05$).
HC, healthy control; PD-MCI, Parkinson's disease with mild cognitive impairment; PD-CN, Parkinson's disease with normal cognition; UPDRS-III off-state, the Movement Disorder Society Unified Parkinson's Disease Rating Scale part III off-state score; LEDD, levodopa-equivalent daily dose; MoCA-total, Montreal Cognitive Assessment; MoCA-language, Montreal Cognitive Assessment subscore related to language function; WMV, total white matter volume; TBV, total brain volume; TIV, total intracranial volume; ns, not significant; NA, not applicable.

3.3. Relationship between R2* and susceptibility

There was a negative correlation between the mean susceptibility and R2* in the splenium of the corpus callosum ($R = -0.343$, $P < 0.01$; Fig. 3a). Compared with the HC and PD-CN groups, the PD-MCI group had significantly higher mean susceptibility, which was close to zero ($P < 0.05$; Fig. 3b), and significantly decreased R2* ($P < 0.01$; Fig. 3c). Moreover, the PD-CN group had higher R2* than the PD-MCI group ($P < 0.05$; Fig. 3c). The WM susceptibility value is negative or close to zero in Fig. 1d, h, and l. The mean susceptibility values for all JHU-WM atlas labels are summarized in Supplementary file 1.

3.4. Correlation of R2* with cognitive performance in patients with PD

The results of voxel-based correlation analyses of MoCA with R2* are shown in Fig. 4a. MoCA showed a significant positive correlation with R2* (FWE-corrected $P < 0.05$) in several WM regions, mainly in the corpus callosum and left WM regions. The significant areas of voxel-based correlation analyses are summarized in Table 3. Fig. 4b, c show the representative regions that provide an overview of the significant correlations of cognition in the genu of the corpus callosum and left fornix with regional R2* values. Among the patients with PD, partial correlation analyses with adjustment for the covariates revealed a positive correlation between R2* and MoCA ($R = 0.335$, $P < 0.05$ in the genu of the corpus callosum and $R = 0.670$, $P < 0.001$ in the left fornix).

4. Discussion

In this study on patients with PD, results of whole-brain voxel-wise R2* relaxometry were compared among the PD-MCI, PD-CN, and HC groups to assess the WM alterations associated with cognitive decline. We found that WM alterations were correlated with cognitive performance in patients with PD. For the first time, we revealed details of WM alteration without detectable regional WM atrophy in PD-MCI using R2* relaxometry and QSM analyses that assessed the microstructural changes in the WM. R2* relaxometry and QSM analyses offered further insight into the pathologic WM changes in PD-MCI.

Ideally, several WM tissue components contribute to the signal. As ARLO assumes a single component, it is necessary to investigate whether the mono-exponential R2* decay model in this study is appropriate, given the multiple compartments and shim variations in the corresponding compartments. The fitting error results for all groups showed the white-noise-like pattern, suggesting that R2* estimated by ARLO is a descriptive parameter that sufficiently explains the data in WM.

Based on the principle of R2* relaxometry analysis, the influence of both iron deposition and microstructural changes in the WM, including demyelination, is inevitable (Paling et al., 2012). If iron deposition occurs secondary to the disease stage conversion from PD-CN to PD-MCI, an increase in the R2* value is predicted. In the present study, however, the correlation analysis between susceptibility and R2* validated that the detectable level of iron deposition was not superimposed on the WM alteration. The significant negative correlation between susceptibility and R2* and the negative mean susceptibility values in all groups suggested that R2* depended only on the myelin content and surrounding microstructural changes. This result also indicates that the susceptibility contrast in WM was mainly dependent on the myelin content and microstructural compartmentalization, not iron deposition. If the contrasts in susceptibility and R2* were driven by iron, we would expect a positive correlation between R2* and susceptibility. Even in

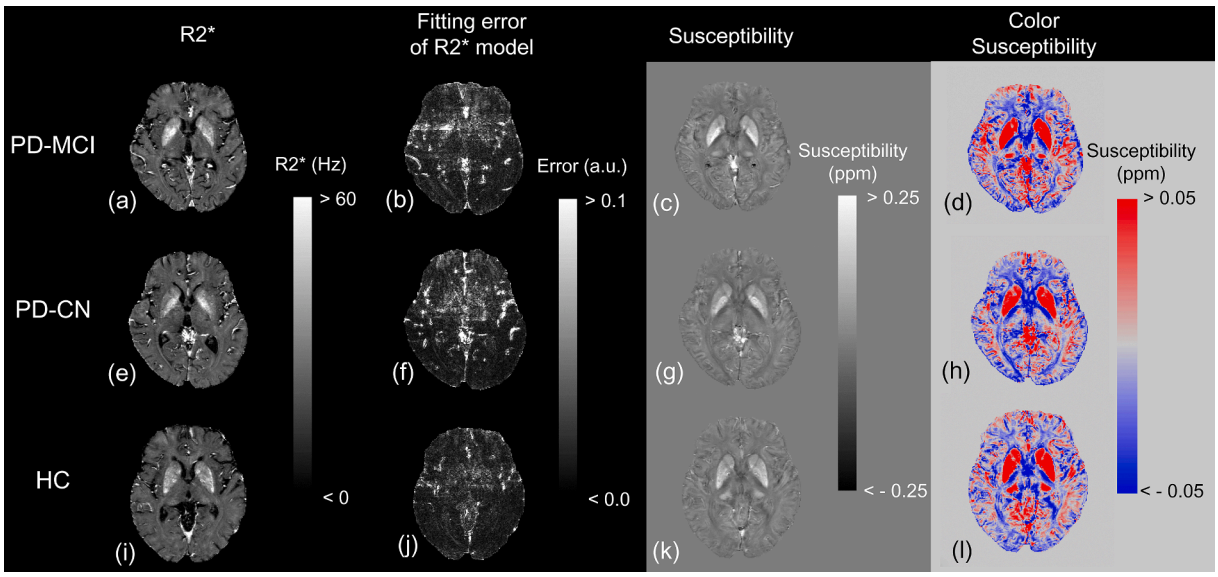

Fig. 1. Representative R2* and susceptibility maps. Representative images of the R2* (a, e, i), fitting error of R2* (b, f, j), susceptibility visualized using a gray scale (c, g, k), and susceptibility visualized using a color scale (d, h, l) map in the PD-MCI, PD-CN, and HC groups, respectively. The fitting error of R2* map indicates a white-noise-like pattern except around the blood vessels. The WM represents a negative or close-to-zero susceptibility value in the color map and was negative or close to zero in all groups. PD-MCI, Parkinson's disease with mild cognitive impairment; PD-CN, Parkinson's disease with normal cognition; HC, healthy control.

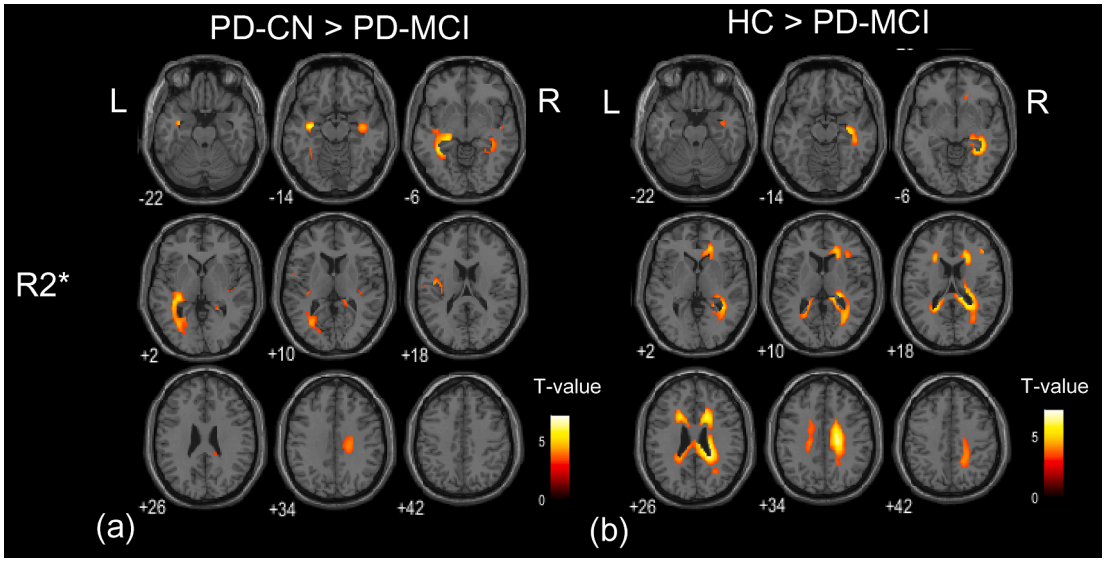

Fig. 2. Results of whole-brain comparison of R2* among the PD-MCI, PD-CN, and HC groups. PD-MCI group has lower R2* in comparison with (a) PD-MCI and (b) HC. The specific anatomical regions are shown in Table 2. PD-MCI, Parkinson's disease with mild cognitive impairment; PD-CN, Parkinson's disease with normal cognition; HC, healthy control.

parts other than the splenium of the corpus callosum, similar assumptions can be made because the mean susceptibility values almost represent negative values or are close to zero. In a few regions showing positive susceptibility values, the volume of interests mapped by the JHU-WM atlas appeared to contain the susceptibility values in WM and slightly iron-rich gray matter owing to the errors occurred by not using spatial smoothing and associated with spatial normalization.

In the voxel-based analysis, the significant R2* decrease in PD-MCI indicated slight demyelination followed by axonal and oligodendrocyte losses and extracellular space enlargement. A relatively low intracellular volume fraction including axons and oligodendrocytes was reported to significantly suggest sparse axonal density in PD with neurocognitive and psychiatric disorders (Andica et al., 2020). Moreover, the extracellular space enlargement can be explained by the increased MD in PD (Bouhrara et al., 2018; Duncan et al., 2016). Our finding was in good agreement with the findings of previous diffusion-based studies on PD (Agosta et al., 2014; Deng et al., 2013). In a study that compared PD-MCI and PD-CN, there were significant decreases in FA in the anterior and superior corona radiata and in the genu and body of the corpus callosum (Agosta et al., 2014). Although the areas with higher MD and/or lower FA varied among studies, these broadly corresponded with our R2* relaxometry analysis. Moreover, the susceptibility WM changes estimated by the QSM analysis were colocalized with the diffusion abnormalities (Guan et al., 2019). This diffusion change might be reflective of the increasing water in the enlarged extracellular space following demyelination and cell death. Eventually, the water susceptibility value becomes close to zero.

Although a DTI study can capture WM alterations by water

Table 2
Whole-brain comparisons of R2* among patients with PD-MCI and PD-CN, and HCs.

Modality	Group comparison	Cluster size (number of voxels)	Peak MNI coordinates			Peak T-value	Anatomical region
			X	Y	Z		
PD-MCI vs. PD-CN							
R*	PD-MCI < PD-CN	3882	−33	−9	−16	7.25	sCC cerebral peduncle, L retrolenticular part of internal capsule, L PTR, L sagittal stratum, L external capsule, L fornix, L SLF, L uncinate fasciculus, L
		993	39	−14	−12	4.73	bCC sCC SCR, R PCR, Rcingulum (cingulate gyrus) , R
		973	21	−24	34	4.21	bCC sCC SCR, R PCR, Rcingulum (cingulate gyrus) , R
PD-MCI vs. HC							
R2*	PD-MCI < HC	17,378	21	−22	32	7.18	gCC bCC sCC anterior and posteriorlimb of internal capsule, R retrolenticular part of internal capsule, R, L ACR, R, L SCR, R, L PCR, R, L PTR, R, L sagittal stratum, R external capsule, Rcingulum (cingulate gyrus) , R, L cingulum (hippocampus) fornix, R SLF, R superior fronto-occipital fasciculus, R, L tapetum, R, L

HC, healthy control; PD-MCI, Parkinson's disease with mild cognitive impairment; PD-CN, Parkinson's disease with normal cognition; gCC, genu of the corpus callosum; bCC, body of the corpus callosum; sCC, splenium of the corpus callosum; PTR, posterior thalamic radiation; ACR, anterior corona radiata; SCR, superior corona radiata; PCR, posterior corona radiata; SLF, superior longitudinal fasciculus; R, right; L, left.

molecular diffusion, the quantitative DTI metrics tend to render indispensable effects from several factors (Beaulieu, 2009). On the other hand, R2* relaxometry analysis combined with QSM aims to distinguish microstructural changes and iron deposition, thereby providing a sensitive and biologically specific measure of the WM. Therefore, the R2* value is a potential candidate imaging marker for PD and can be added to DTI analysis to investigate the details of WM alteration in neurodegenerative diseases. By comparing PD-MCI and PD-CN, we have proved that the WM alterations associated with cognitive decline depended on demyelination in patients with PD. Nevertheless, the pathological meaning of the WM alteration revealed by the R2* value remains elusive. The WM alteration, as indicated by the decrease in R2*, might be due to demyelination followed by Wallerian degeneration (Benjamini et al., 2020; Tagliaferro and Burke, 2016). This degeneration is caused by injury or neural cell death due to neurotoxin exposure caused by α-synuclein, which contributes to PD pathology (Burke and O'Malley, 2013). Widespread α-synuclein aggregation promoted by iron accumulation was observed in a previous QSM study targeting to gray matter (Uchida et al., 2019). The finding that R2* decreased in PD-MCI across many WM regions is consistent with the previous study.

In this study, the association of R2* changes with cognitive performance in some WM regions might be appropriate for the early evaluation of cognitive decline in PD. The genu of the corpus callosum, in which MoCA was found to have significant correlation with R2*, is associated with the memory, attention, language, visuospatial, and executive functions of the cognitive domain in diffusion MRI (Bledsoe et al., 2018). The corpus callosum is the largest commissural WM bundle of the brain that connects both hemispheres and plays essential roles in the interhemispheric transfer of information and cognitive and sensory integrations. The correlation of MoCA with R2* in some corpus callosum regions was reflective of cognitive dysfunction in PD-MCI. Moreover, the fornix result has also been suggested to underlie cognitive deficits in PD. Degeneration of fornix formed fornix-hippocampal circuit leads to the episodic memory consolidation (Fletcher et al., 2013; Zhuang et al., 2012). The marked laterality of the correlation between R2* and MoCA has been found. This left-hemispheric symmetry may partly be well reflective of the functional dominance for language processing, supported by the language-related MoCA subscore results. This result extended prior findings and was reasonable to explain the strong relationships among demyelination, axonal and oligodendrocyte losses, and extracellular water increase owing to extracellular space enlargement and cognitive performance. As the R2* value was correlated with the decline of cognitive function, the R2* value may potentially be an emerging biomarker for assessing the progression of cognitive impairment in patients with PD, even at an earlier stage.

R2* relaxometry analysis can reveal widespread WM abnormalities, such as slight demyelination and intra- and extracellular space changes, without complicated models, unlike diffusion-based analysis. The extracted details of WM alterations highlighted to coincide with the findings in diffusion-based analysis with few inconsistencies. Therefore,

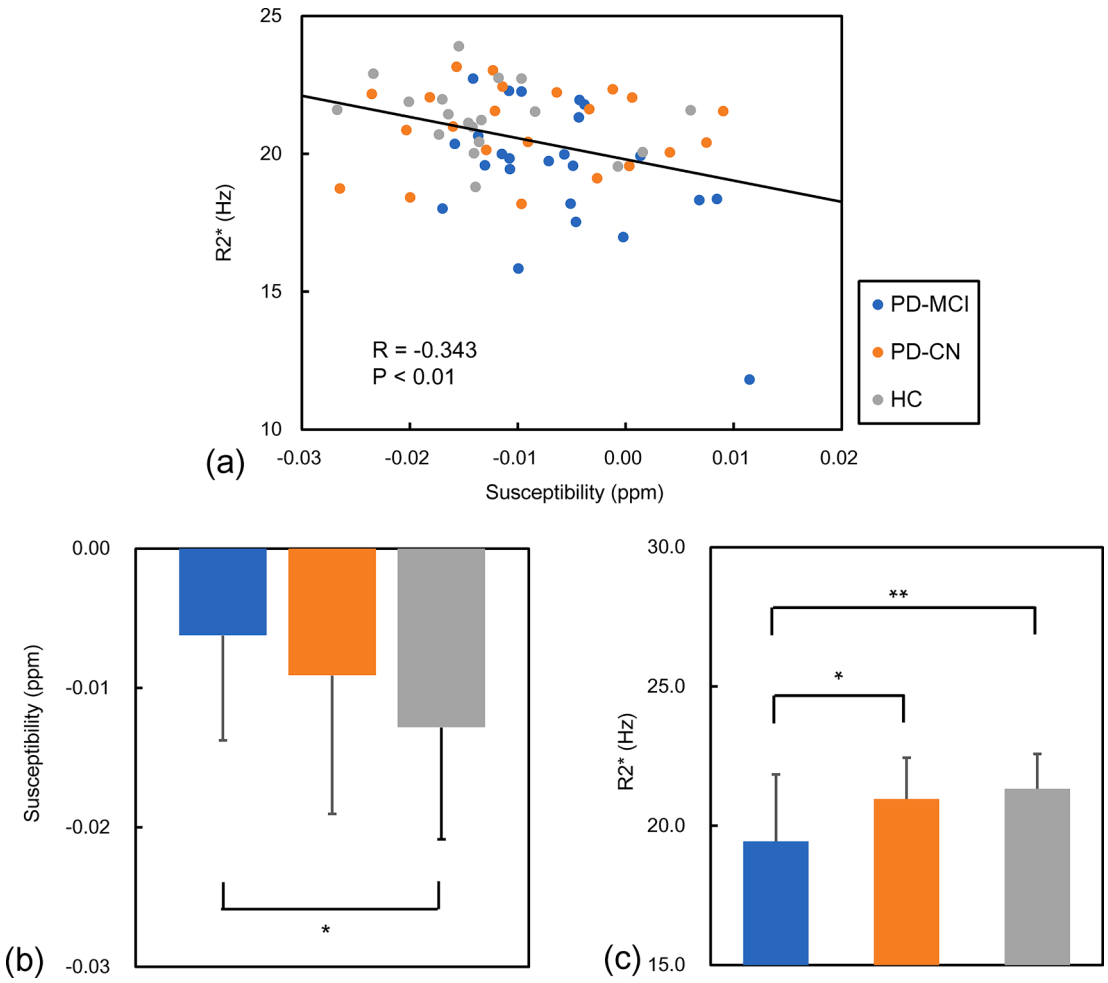

Fig. 3. Relationship between R2* and susceptibility in the sCC. R2* shows a significantly negative correlation with (a) susceptibility ($R = -0.343$, $P < 0.01$). Compared with the HC group, the PD-MCI group has significantly increased mean susceptibility (b, $P < 0.05$) and significantly decreased R2* (c, $P < 0.01$). *; $P < 0.05$, **; $P < 0.01$ sCC, splenium of the corpus callosum; PD-MCI, Parkinson's disease with mild cognitive impairment; PD-CN, Parkinson's disease with normal cognition; HC, healthy control.

R2* relaxometry analysis reached higher spatial resolution might provide auxiliary imaging biomarkers in neurodegenerative diseases, such as PD, besides diffusion-based metrics. Moreover, the dual analyses of R2* relaxometry in WM and QSM in gray matter on a single dataset acquired from mGRE might allow boosting of the more accurate early evaluation of cognitive decline in patients with PD, because the susceptibility changes in the cortical cortex and basal ganglia in PD-MCI were reported using QSM analysis (Guan et al., 2017; Uchida et al., 2020).

There are several limitations to this study. In the signal correction of mGRE, voxels shaped completely rectangular were assumed. The voxel is actually a sinc-like shape due to the intervoxel signal leakage and signal contamination to the surrounding voxels (i.e., Gibbs ringing artifact) (Bashir and Yablonskiy, 2006). To settle this problem, sophisticated solutions were proposed with the signal correction using voxel-spread functions (VSF) (Yablonskiy et al., 2013). As the signal correction method is different from the ideal methods, their approximation effects might be included in the results of the R2* relaxometry analysis. However, the signal correction factors at TE in several voxels in the WM regions, including the corpus callosum were found to be approximately 0.99 – 1.0 using our method and the VSF method (data not shown). This implies that the difference in correction methods made almost no contribution to the results of this study since the WM is located away from the air-tissue boundary with a strong macroscopic field inhomogeneity. The current cross-sectional analysis relates to the limitations of the smaller patient number in the subgroups in this study. Moreover, a diagnosis of PD-MCI was made according to the proposed MDS Task Force Level 1 criteria, but we should have performed the Level 2 criteria ideally. It provides a preliminary assessment of the relationships between R2* and cognitive impairment. Additional longitudinal studies are warranted to confirm the novel insights obtained from our research. Use of head orientations against a main static field as covariates remains controversial, because the head orientations do not have an exactly linear influence on R2* (Kor et al., 2019; Sedlacik et al., 2014). However, there were no significant differences among the groups. Hence, the effects of head orientation on R2* value were minimal in this study. Despite these limitations, R2* relaxometry analysis can successfully depict differences in PD-MCI and PD-CN and represent the correlation between R2* values and cognitive function.

5. Conclusion

R2* relaxometry analysis of WM microstructural changes can provide further biological insights on demyelination and changes in the surrounding environment, as supported by the QSM results demonstrating that the change in R2* was not due to a reduction in iron. These findings highlight the potential of R2* relaxometry analysis for early evaluation of cognitive decline in patients with PD.

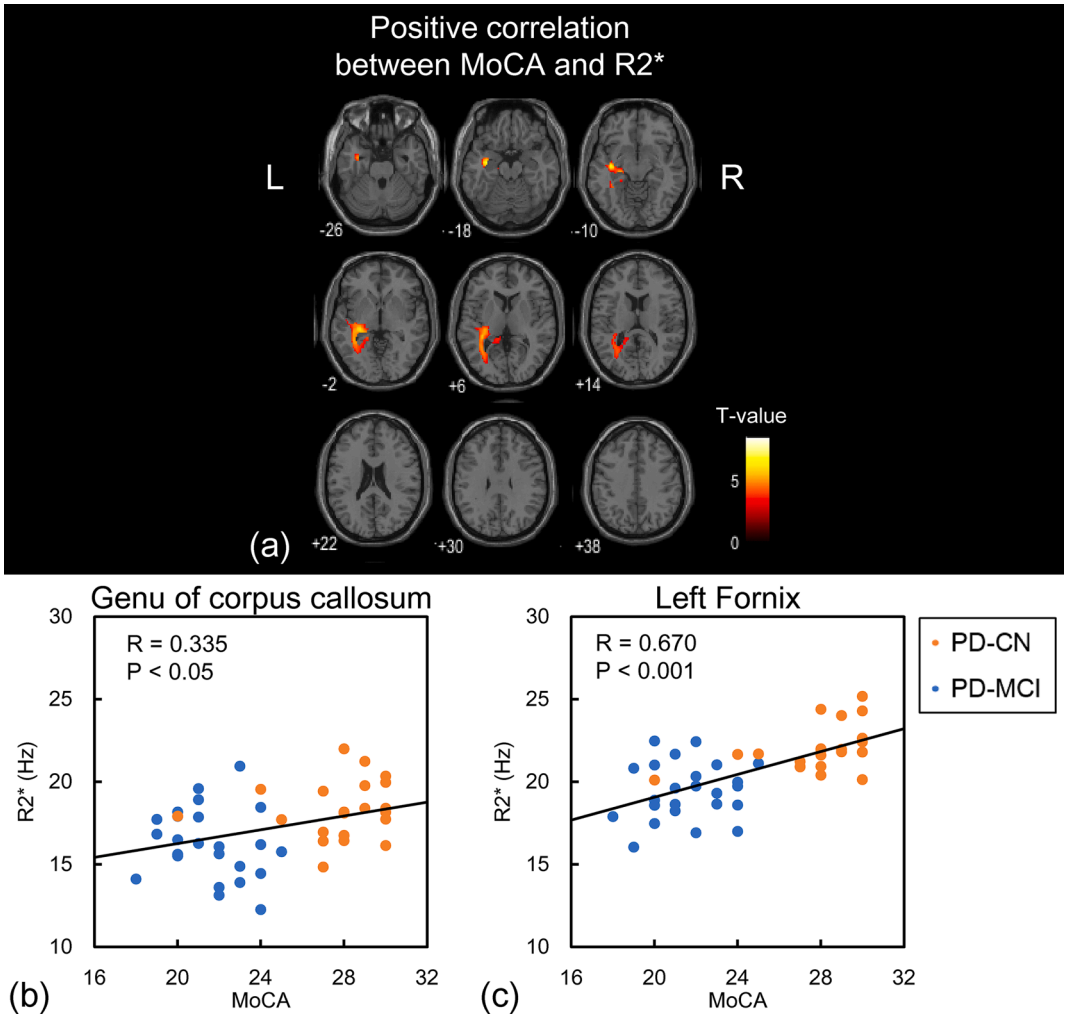

Fig. 4. *Upper panel:* (a) Result of whole-brain analysis of the correlation of MoCA with R2* in patients with PD. The specific anatomical regions are shown in Table 3. *Lower panel:* Relationships between MoCA and R2*. MoCA shows a positive correlation with R2*. The relationship between R2* and MoCA in the (b) genu of the corpus callosum and (c) left fornix are shown. MoCA, Montreal Cognitive Assessment; PD, Parkinson's disease.

Table 3
Whole-brain correlation analyses of MoCA with R2* in patients with PD.

			Peak MNI coordinates				
Modality	Contrast	Cluster size (number of voxels)	X	Y	Z	Peak T-value	Anatomical region
R2*	Positive correlation	4525	−36	−12	−14	8.44	sCC cerebral peduncle, L posterior limb of internal capsule, L retrolenticular part of internal capsule, L PCR, L PTR, L sagittal stratum, L external capsule, Lcingulum (hippocampus) , L fornix, L SLF, L uncinate fasciculus, L tapetum, L

PD, Parkinson's disease; gCC, genu of the corpus callosum; sCC, splenium of the corpus callosum; PTR, posterior thalamic radiation; ACR, anterior corona radiata; SCR, superior corona radiata; PCR, posterior corona radiata; SLF, superior longitudinal fasciculus; R, right; L, left.

6. Ethics statement

This study was approved by the institutional review board of Nagoya City University Hospital and Nagoya University.

Funding

This work was supported by KAKENHI, Grant-in-Aid for Scientific Research on Innovative Areas, "Willdynamics" [grant number 16H06403]; the Japan Society for the Promotion of Science (JSPS)

KAKENHI [grant number 15K09355] (YU) and KAKENHI [grant number 17K15805] (HK).

CRediT authorship contribution statement

Hirohito Kan: Conceptualization, Methodology, Software, Formal analysis, Investigation, Data curation, Writing – original draft, Funding acquisition. **Yuto Uchida:** Conceptualization, Formal analysis, Investigation, Data curation, Supervision, Resources, Writing – review & editing, Funding acquisition. **Yoshino Ueki:** Conceptualization, Supervision, Resources, Writing – review & editing, Funding acquisition. **Nobuyuki Arai:** Data curation, Investigation. **Satoshi Tsubokura:** Data curation, Investigation. **Hiroshi Kunitomo:** . **Harumasa Kasai:** Data curation, Investigation. **Kiminori Aoyama:** Supervision, Writing – review & editing. **Noriyuki Matsukawa:** Supervision, Writing – review & editing. **Yuta Shibamoto:** Supervision, Writing – review & editing.

Declaration of Competing Interest

The authors declare that they have no known competing financial interests or personal relationships that could have appeared to influence the work reported in this paper.

Appendix A. Supplementary data

Supplementary data to this article can be found online at https://doi.org/10.1016/j.nicl.2022.102938.

References

Agosta, F., Canu, E., Stefanova, E., Sarro, L., Tomić, A., Špica, V., Comi, G., Kostić, V.S., Filippi, M., 2014. Mild cognitive impairment in Parkinson's disease is associated with a distributed pattern of brain white matter damage. Hum. Brain Mapp. 35 (5), 1921–1929.

Alonso-Ortiz, E., Levesque, I.R., Paquin, R., Pike, G.B., 2017. Field inhomogeneity correction for gradient echo myelin water fraction imaging. Magn. Reson. Med. 78 (1), 49–57.

Andica, C., Kamagata, K., Hatano, T., Saito, Y., Uchida, W., Ogawa, T., Takeshige-Amano, H., Hagiwara, A., Murata, S., Oyama, G., Shimo, Y., Umemura, A., Akashi, T., Wada, A., Kumamaru, K.K., Hori, M., Hattori, N., Aoki, S., 2020. Neurocognitive and psychiatric disorders-related axonal degeneration in Parkinson's disease. J. Neurosci. Res. 98 (5), 936–949.

Ashburner, J., 2007. A fast diffeomorphic image registration algorithm. Neuroimage 38 (1), 95–113.

Bagher-Ebadian, H., Jiang, Q., Ewing, J.R., 2008. A modified Fourier-based phase unwrapping algorithm with an application to MRI venography. J. Magn. Reson. Imag. JMRI 27 (3), 649–652.

Bashir, A., Yablonskiy, D.A., 2006. Natural linewidth chemical shift imaging (NL-CSI). Magn. Reson. Med. 56 (1), 7–18.

Beaulieu, C., 2009. Chapter 6. The biological basis of diffusion anisotropy. In: Johansen-Berg, H., Behrens, T.E.J. (Eds.), Diffusion MRI. Academic Press, San Diego, pp. 105–126.

Benjamini, D., Hutchinson, E.B., Komlosh, M.E., Comrie, C.J., Schwerin, S.C., Zhang, G., Pierpaoli, C., Basser, P.J., 2020. Direct and specific assessment of axonal injury and spinal cord microenvironments using diffusion correlation imaging. Neuroimage 221, 117195. https://doi.org/10.1016/j.neuroimage.2020.117195.

Bledsoe, I.O., Stebbins, G.T., Merkitch, D., Goldman, J.G., 2018. White matter abnormalities in the corpus callosum with cognitive impairment in Parkinson disease. Neurology 91 (24), e2244–e2255.

Bouhrara, M., Reiter, D.A., Bergeron, C.M., Zukley, L.M., Ferrucci, L., Resnick, S.M., Spencer, R.G., 2018. Evidence of demyelination in mild cognitive impairment and dementia using a direct and specific magnetic resonance imaging measure of myelin content. Alzheimers Dement 14 (8), 998–1004.

Burke, R.E., O'Malley, K., 2013. Axon degeneration in Parkinson's disease. Exp. Neurol. 246, 72–83.

Dahnke, H., Schaeffter, T., 2005. Limits of detection of SPIO at 3.0 T usingT2* relaxometry. Magn. Reson. Med. 53 (5), 1202–1206.

Dalrymple-Alford, J.C., MacAskill, M.R., Nakas, C.T., Livingston, L., Graham, C., Crucian, G.P., Melzer, T.R., Kirwan, J., Keenan, R., Wells, S., Porter, R.J., Watts, R., Anderson, T.J., 2010. The MoCA: well-suited screen for cognitive impairment in Parkinson disease. Neurology 75 (19), 1717–1725.

Deistung, A., Schweser, F., Reichenbach, J.R., 2017. Overview of quantitative susceptibility mapping. NMR Biomed. 30, e3569.

Deng, B., Zhang, Y., Wang, L., Peng, K., Han, L., Nie, K., Yang, H., Zhang, L.i., Wang, J., 2013. Diffusion tensor imaging reveals white matter changes associated with cognitive status in patients with Parkinson's disease. Am. J. Alzheimers Dis. Other Demen. 28 (2), 154–164.

Du, Y.P., Chu, R., Hwang, D., Brown, M.S., Kleinschmidt-DeMasters, B.K., Singel, D., Simon, J.H., 2007. Fast multislice mapping of the myelin water fraction using multicompartment analysis of T2* decay at 3T: a preliminary postmortem study. Magn. Reson. Med. 58 (5), 865–870.

Duncan, G.W., Firbank, M.J., Yarnall, A.J., Khoo, T.K., Brooks, D.J., Barker, R.A., Burn, D.J., O'Brien, J.T., 2016. Gray and white matter imaging: a biomarker for cognitive impairment in early Parkinson's disease? Mov. Disord. 31 (1), 103–110.

Fazekas, F., Chawluk, J.B., Alavi, A., Hurtig, H.I., Zimmerman, R.A., 1987. MR signal abnormalities at 1.5 T in Alzheimer's dementia and normal aging. AJR Am. J. Roentgenol. 149 (2), 351–356.

Fletcher, E., Raman, M., Huebner, P., Liu, A., Mungas, D., Carmichael, O., DeCarli, C., 2013. Loss of fornix white matter volume as a predictor of cognitive impairment in cognitively normal elderly individuals. JAMA Neurol 70 (11), 1389. https://doi.org/10.1001/jamaneurol.2013.3263.

Fortier, V., Levesque, I.R., 2018. Phase processing for quantitative susceptibility mapping of regions with large susceptibility and lack of signal. Magn. Reson. Med. 79 (6), 3103–3113.

Georgiopoulos, C., Warntjes, M., Dizdar, N., Zachrisson, H., Engstrom, M., Haller, S., Larsson, E.M., 2017. Olfactory impairment in parkinson's disease studied with diffusion tensor and magnetization transfer imaging. J. Parkinsons Dis. 7, 301–311.

Guan, X., Huang, P., Zeng, Q., Liu, C., Wei, H., Xuan, M., Gu, Q., Xu, X., Wang, N., Yu, X., Luo, X., Zhang, M., 2019. Quantitative susceptibility mapping as a biomarker for evaluating white matter alterations in Parkinson's disease. Brain Imaging Behav. 13 (1), 220–231.

Guan, X., Xuan, M., Gu, Q., Huang, P., Liu, C., Wang, N., Xu, X., Luo, W., Zhang, M., 2017. Regionally progressive accumulation of iron in Parkinson's disease as measured by quantitative susceptibility mapping. NMR Biomed. 30, e3489.

Guimarães, R.P., Campos, B.M., de Rezende, T.J., Piovesana, L., Azevedo, P.C., Amato-Filho, A.C., Cendes, F., D'Abreu, A., 2018. Is diffusion tensor imaging a good biomarker for early Parkinson's disease? Front. Neurol. 9 https://doi.org/10.3389/fneur.2018.00626.

Hattori, T., Orimo, S., Aoki, S., Ito, K., Abe, O., Amano, A., Sato, R., Sakai, K., Mizusawa, H., 2012. Cognitive status correlates with white matter alteration in Parkinson's disease. Hum. Brain Mapp. 33 (3), 727–739.

Hwang, D., Kim, D.-H., Du, Y.P., 2010. In vivo multi-slice mapping of myelin water content using T2* decay. NeuroImage 52 (1), 198–204.

Kamagata, K., Motoi, Y., Tomiyama, H., Abe, O., Ito, K., Shimoji, K., Suzuki, M., Hori, M., Nakanishi, A., Sano, T., Kuwatsuru, R., Sasai, K., Aoki, S., Hattori, N., 2013. Relationship between cognitive impairment and white-matter alteration in Parkinson's disease with dementia: tract-based spatial statistics and tract-specific analysis. Eur. Rad. 23 (7), 1946–1955.

Kan, H., Arai, N., Kasai, H., Kunitomo, H., Hirose, Y., Shibamoto, Y., 2017. Quantitative susceptibility mapping using principles of echo shifting with a train of observations sequence on 1.5T MRI. Magn. Reson. Imaging 42, 37–42.

Kan, H., Kasai, H., Arai, N., Kunitomo, H., Hirose, Y., Shibamoto, Y., 2016. Background field removal technique using regularization enabled sophisticated harmonic artifact reduction for phase data with varying kernel sizes. Magn. Reson. Imaging 34 (7), 1026–1033.

Kan, H., Uchida, Y., Arai, N., Ueki, Y., Aoki, T., Kasai, H., Kunitomo, H., Hirose, Y., Matsukawa, N., Shibamoto, Y., 2020. Simultaneous voxel-based magnetic susceptibility and morphometry analysis using magnetization-prepared spoiled turbo multiple gradient echo. NMR Biomed. 33 (5) https://doi.org/10.1002/nbm.v33.510.1002/nbm.4272.

Kehagia, A.A., Barker, R.A., Robbins, T.W., 2010. Neuropsychological and clinical heterogeneity of cognitive impairment and dementia in patients with Parkinson's disease. Lancet Neurol. 9 (12), 1200–1213.

Kim, H.J., Kim, S.J., Kim, H.S., Choi, C.G., Kim, N., Han, S., Jang, E.H., Chung, S.J., Lee, C.S., 2013. Alterations of mean diffusivity in brain white matter and deep gray matter in Parkinson's disease. Neurosci. Lett. 550, 64–68.

Kor, D., Birkl, C., Ropele, S., Doucette, J., Xu, T., Wiggermann, V., Hernández-Torres, E., Hametner, S., Rauscher, A., 2019. The role of iron and myelin in orientation dependent R2 (*) of white matter. NMR Biomed. e4092. https://doi.org/10.1002/nbm.4092.

Lanskey, J.H., McColgan, P., Schrag, A.E., Acosta-Cabronero, J., Rees, G., Morris, H.R., Weil, R.S., 2018. Can neuroimaging predict dementia in Parkinson's disease? Brain 141, 2545–2560.

Laule, C., Kozlowski, P., Leung, E., Li, D.K., Mackay, A.L., Moore, G.R., 2008. Myelin water imaging of multiple sclerosis at 7 T: correlations with histopathology. NeuroImage 40, 1575–1580.

Li, W., Wang, N., Yu, F., Han, H., Cao, W., Romero, R., Tantiwongkosi, B., Duong, T.Q., Liu, C., 2015. A method for estimating and removing streaking artifacts in quantitative susceptibility mapping. Neuroimage 108, 111–122.

Litvan, I., Aarsland, D., Adler, C.H., Goldman, J.G., Kulisevsky, J., Mollenhauer, B., Rodriguez-Oroz, M.C., Tröster, A.I., Weintraub, D., 2011. MDS Task Force on mild cognitive impairment in Parkinson's disease: critical review of PD-MCI. Mov. Disord. 26 (10), 1814–1824.

Litvan, I., Goldman, J.G., Tröster, A.I., Schmand, B.A., Weintraub, D., Petersen, R.C., Mollenhauer, B., Adler, C.H., Marder, K., Williams-Gray, C.H., Aarsland, D., Kulisevsky, J., Rodriguez-Oroz, M.C., Burn, D.J., Barker, R.A., Emre, M., 2012. Diagnostic criteria for mild cognitive impairment in Parkinson's disease: movement disorder society task force guidelines. Mov. Disord. 27 (3), 349–356.

Mori, S., Oishi, K., Jiang, H., Jiang, L.i., Li, X., Akhter, K., Hua, K., Faria, A.V., Mahmood, A., Woods, R., Toga, A.W., Pike, G.B., Neto, P.R., Evans, A., Zhang, J., Huang, H., Miller, M.I., van Zijl, P., Mazziotta, J., 2008. Stereotaxic white matter atlas based on diffusion tensor imaging in an ICBM template. Neuroimage 40 (2), 570–582.

Muslimovic, D., Post, B., Speelman, J.D., Schmand, B., 2005. Cognitive profile of patients with newly diagnosed Parkinson disease. Neurology 65, 1239–1245.
Özbay, P.S., Deistung, A., Feng, X., Nanz, D., Reichenbach, J.R., Schweser, F., 2017. A comprehensive numerical analysis of background phase correction with V-SHARP. NMR Biomed. 30, e3550.
Paling, D., Tozer, D., Wheeler-Kingshott, C., Kapoor, R., Miller, D.H., Golay, X., 2012. Reduced R2' in multiple sclerosis normal appearing white matter and lesions may reflect decreased myelin and iron content. J. Neurol. Neurosurg. Psychiatry 83, 785–792.
Pei, M., Nguyen, T.D., Thimmappa, N.D., Salustri, C., Dong, F., Cooper, M.A., Li, J., Prince, M.R., Wang, Y., 2015. Algorithm for fast monoexponential fitting based on auto-regression on linear operations (ARLO) of data. Magn. Reson. Med. 73, 843–850.
Rektor, I., Svátková, A., Vojtíšek, L., Zikmundová, I., Vaníček, J., Király, A., Szabó, N., 2018. White matter alterations in Parkinson's disease with normal cognition precede grey matter atrophy. PLoS ONE 13, e0187939.
Ridgway, G.R., Omar, R., Ourselin, S., Hill, D.L., Warren, J.D., Fox, N.C., 2009. Issues with threshold masking in voxel-based morphometry of atrophied brains. Neuroimage 44, 99–111.
Sedlacik, J., Boelmans, K., Löbel, U., Holst, B., Siemonsen, S., Fiehler, J., 2014. Reversible, irreversible and effective transverse relaxation rates in normal aging brain at 3T. Neuroimage 84, 1032–1041.
Song, R., Lin, W., Chen, Q., Asakura, T., Wehrli, F.W., Song, H.K., 2008. Relationships between MR transverse relaxation parametersR*2, R2andR′2 and hepatic iron content in thalassemic mice at 1.5 T and 3 T. NMR Biomed. 21, 574–580.
Tagliaferro, P., Burke, R.E., 2016. Retrograde axonal degeneration in parkinson disease. J. Parkinsons Dis. 6, 1–15.
Uchida, Y., Kan, H., Sakurai, K., Arai, N., Kato, D., Kawashima, S., Ueki, Y., Matsukawa, N., 2019. Voxel-based quantitative susceptibility mapping in Parkinson's disease with mild cognitive impairment. Mov. Disord. 34, 1164–1173.
Uchida, Y., Kan, H., Sakurai, K., Inui, S., Kobayashi, S., Akagawa, Y., Shibuya, K., Ueki, Y., Matsukawa, N., 2020. Magnetic susceptibility associates with dopaminergic deficits and cognition in Parkinson's disease. Mov. Disord. 35, 1396–1405.
Wu, B., Li, W., Avram, A.V., Gho, S.-M., Liu, C., 2012. Fast and tissue-optimized mapping of magnetic susceptibility and T2* with multi-echo and multi-shot spirals. NeuroImage 59, 297–305.
Yablonskiy, D.A., Sukstanskii, A.L., Luo, J., Wang, X., 2013. Voxel spread function method for correction of magnetic field inhomogeneity effects in quantitative gradient-echo-based MRI. Magn. Reson. Med. 70, 1283–1292.
Zarkali, A., McColgan, P., Leyland, L.A., Lees, A.J., Rees, G., Weil, R.S., 2020. Fiber-specific white matter reductions in Parkinson hallucinations and visual dysfunction. Neurology 94, e1525–e1538.
Zheng, Z., Shemmassian, S., Wijekoon, C., Kim, W., Bookheimer, S.Y., Pouratian, N., 2014. DTI correlates of distinct cognitive impairments in Parkinson's disease. Hum. Brain Mapp. 35, 1325–1333.
Zhuang, L., Sachdev, P.S., Trollor, J.N., Kochan, N.A., Reppermund, S., Brodaty, H., Wen, W., 2012. Microstructural white matter changes in cognitively normal individuals at risk of amnestic MCI. Neurology 79, 748–754.